Journal of Power Sources 195 (2010) 7196–7201

Contents lists available at ScienceDirect

Journal of Power Sources

journal homepage: www.elsevier.com/locate/jpowsour

A liquid electrolyte alkaline direct 2-propanol fuel cell

Matthew E.P. Markiewicz, Steven H. Bergens*

Department of Chemistry, University of Alberta, Edmonton, Alberta T6G 2G2, Canada

ARTICLE INFO

Article history:
Received 9 April 2010
Received in revised form 6 May 2010
Accepted 7 May 2010
Available online 15 May 2010

Keywords:
Direct alcohol fuel cell
2-Propanol
Methanol
Alkaline

ABSTRACT

Prototype alkaline direct 2-propanol fuel cells (AD2PFCs) using commercial Pt/C electrodes and hardware, and a liquid electrolyte, were constructed and compared to the 3-dimensional current–time–potential profiles for the 3-electrode oxidation of 2-propanol. A substantial current maximum occurs at low potentials and is attributed to a change in the mechanism of 2-propanol oxidation. This mechanism change influenced the stability of the AD2PFC; when the cell was polarized to a lower cell voltage limit of 0.5 V, stable and relatively high power densities are achieved. When the cell was polarized to a lower cell voltage limit of 0 V, unstable and only marginally higher power densities were observed. A maximum power density of 22.3 mW mg_{Pt}^{-1} was achieved, and most of the cell polarization occurred at the cathode.

1. Introduction

We report an electrically efficient prototype alkaline direct 2-propanol fuel cell (AD2PFC) operating with commercial platinum electrodes and a liquid electrolyte. The high volumetric and gravimetric energy densities of alcohols make direct alcohol fuel cells (DAFCs) a promising power source for portable electronic devices. Further, the ease and simplicity of handling liquid alcohol fuels are an attractive alternative to hydrogen transport and storage. DAFCs, however, typically operate with lower performances than fuel cells operating on hydrogen. The causes for this lower performance [1] are slow alcohol oxidation kinetics at the anode and crossover of alcohol and water from the anode to the cathode. Crossover is due to the solubility of the alcohol in the electrolyte and is driven by the concentration gradient and electroosmosis; it reduces the cathode potential, causes cathode flooding, and it reduces the fuel efficiency through alcohol evaporation. Research on DAFCs using acidic electrolytes, mainly Nafion®, is more established than research on alkaline DAFCs (ADAFCs). The potential advantages of an alkaline over an acidic electrolyte include [1,2]: first, the flow of charge carriers is from the cathode to the anode, impeding alcohol crossover from the anode to the cathode; second, the oxidation of alcohols and the reduction of oxygen are faster in base; and third, the library of materials that do not corrode is larger in base, allowing for cheaper catalysts layers and cell components [3]. These advantages have, in part, caused a considerable increase in recent ADAFC research activity.

The ADAFC literature has been recently reviewed [2]. By far, the most studied alcohols are methanol (ADMFC) [4–15] and ethanol (ADEFC) [15–22]. The ADMFC oxidation products are a mixture of carbon dioxide and formic acid over platinum [3], or palladium [15] electrocatalysts. The ADEFC products are acetic acid and acetaldehyde over platinum [3], and acetic acid over palladium [15,16]. These products react in non-electrochemical acid/base reactions to consume hydroxide and thus require the use of hydroxide-alcohol fuel mixtures to replenish the hydroxide consumed at the anode.

Several groups [23–27], including our own [28–30], have studied 2-propanol as an alternative to methanol or ethanol in ADAFCs. These studies propose that dehydrogenation of 2-propanol to acetone occurs at low potentials (Scheme 1), and that a slower oxidation to form CO_2 occurs at higher potentials. Unlike carbon dioxide, formic acid, and acetic acid, acetone does not react in irreversible stoichiometric side reactions with hydroxide and thus does not require added base. In 3-electrode experiments, the platinum catalyzed electro-oxidation of 2-propanol to acetone provides relatively high stabilized current densities at low anode potentials [29]. The activity of platinum at these potentials is enhanced by ruthenium [30] or nickel [28]. Over palladium, the apparent activation energy for 2-propanol oxidation is lower than ethanol at moderate potentials [24], and its activity is enhanced by gold [23] or platinum [25]. Only one report of an operating AD2PFC can be found in the literature [31]. Using a PtRu anode (2 mg cm^{-2}), Yang et al. reported a maximum power density of 5.46 mW cm^{-2} for the AD2PFC, and 9.25 and 8.00 mW cm^{-2} for the same cell operating on methanol and ethanol, respectively.

The goal of this study was to construct a prototype AD2PFC with a liquid KOH electrolyte, 100% alcohol fuel, and commercial platinum electrodes. The performance characteristics of the cell were

* Corresponding author. Tel.: +1 780 492 9703; fax: +1 780 492 8231.
E-mail address: steve.bergens@ualberta.ca (S.H. Bergens).

0378-7753/$ – see front matter © 2010 Elsevier B.V. All rights reserved.
doi:10.1016/j.jpowsour.2010.05.017

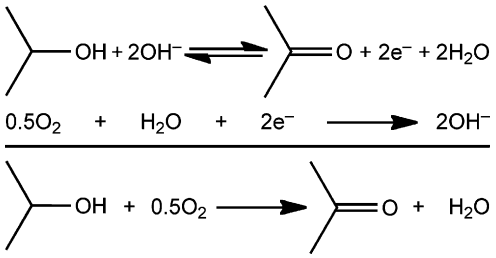

Scheme 1.

correlated to the ex situ activity and stability of 2-propanol oxidation, using 3-dimensional current–potential–time profiles.

2. Experimental

2.1. General

Nitrogen (Praxair, prepurified), hydrogen (Praxair, prepurified), oxygen (Praxair), $KMnO_4$ (Fisher, ACS grade) and KOH (Caledon, reagent grade) were used as received. Water from an in-house distilled water line was distilled a second time, and then distilled from alkaline $KMnO_4$. 2-Propanol (Fisher Scientific, suitable for electronic use) and methanol (Fisher, ACS grade) were freshly distilled before use. ESNS electrodes (silver plated nickel screen, 0.6 mg cm^{-2} platinum loading using 10% platinum on Vulcan XC-72 or 1.5 mg cm^{-2} platinum loading using 20% platinum on Vulcan XC-72) were pre-treated as outlined in Sections 2.2 and 2.3. All potentials are reported vs. SHE unless stated otherwise. Measurements are not iR compensated.

2.2. 3-Electrode experiments

Electrochemical experiments were performed using the setup described previously [29]. The working electrode was a 1 cm^2 ESNS electrode (0.6 mg_{Pt} cm^{-2} or 1.5 mg_{Pt} cm^{-2}); it was conditioned in 1 M KOH at 60 °C by potential cycling between −0.5 V and 0.5 V vs. RHE at 5 mV s^{-1} until a stable response was achieved (∼60 cycles). The electrode was then cleaned in 3% H_2O_2 at 0 °C for several hours, and then slowly warmed to room temperature until all the peroxide had been consumed. The electrode was immersed in a 1 M KOH/1 M 2-propanol electrolyte at 60 °C and held at −0.928 V vs. SHE for 5 min to reduce the electrocatalyst surface. Potential step experiments were then performed for 15 min, with 2 min conditioning steps between potentiostatic experiments ($E_{conditioning}$ = −0.928 V vs. SHE).

2.3. Fuel cell experiments

Commercial fuel cell hardware (QuickCell^{TM} QC200) was purchased from Astris Energi (Fig. 1). Electrodes with a 5 cm^2 geometric area were constructed by mounting ESNS electrodes (0.6 mg_{Pt} cm^{-2} or 1.5 mg_{Pt} cm^{-2}) in Teflon frames that were fitted with a current collecting nickel wire. ∼200 mL of 5 M KOH electrolyte was maintained at 70 °C within an external reservoir and was recirculated using an N_2 gas lift pump at bubbler rate. The volume of electrolyte between the electrodes was ∼7.5 mL, and the volume of the anode/cathode chambers was ∼5.0 mL. When the cell was operated on alcohol fuels the electrolyte was drained from an outlet between the anode and cathode (2.5 mL min^{-1}) and fresh electrolyte was periodically added to the reservoir. Electrodes were first conditioned under hydrogen by sweeping between −0.5 V and 0.5 V vs. RHE at 5 mV s^{-1} until a stable response was achieved (∼60 cycles). Experiments were performed using dry hydrogen (600 sccm, RT), 100% methanol (0.5 mL min^{-1}, RT), 100% 2-propanol (0.5 mL min^{-1}, RT), and dry oxygen (300 sccm, RT). Polarization curves were collected by stepping the current density using a logarithmic scale; the cell potential was allowed to equilibrate for 30 s at each current density before recording the cell potential.

3. Results and discussion

Fig. 2(a) shows the 3-dimensional current–time–potential (j–t–E) profile for the electro-oxidation of 2-propanol using a low loading commercial platinum electrode (ESNS, 0.6 mg cm^{-2} Pt/C). Fig. 2(b) shows the current observed at 0.5 min, 3 min, and 15 min vs. the applied potential. The electrode was first reduced electrochemically by evolving hydrogen at −0.928 V vs. SHE for 2 min, and then held at the desired experimental potential for 15 min. The resulting current–time transients were then plotted against the applied potential to generate the 3-dimensional profile. The current maximum at −0.578 V vs. SHE (12.9 mA cm^{-2} or 21.5 mA mg_{Pt}^{-1} at 15 min) is consistent with those we reported using platinum gauzes [29] and unsupported nanoparticles [30]. To our knowledge, they are the highest reported stabilized current densities for the oxidation of an alcohol at low anode potentials, e.g., at 0.250 V above the reversible hydrogen electrode (RHE = −0.828 V vs. SHE). We have previously shown that this low-potential current maximum occurs near the onset of acetone oxidation [29,30]; herein we also show that this maximum is accompanied by a dramatic change in the stability of the current transients. Fig. 3 illustrates this change by plotting the percentage of the current lost over the final 10 min of the electro-oxidation [$((j_5 - j_{15})/j_{15}) \times 100$] vs. the step potential. The magnitude of the current density at each potential step (j_{15}) is also supplied for comparison. A pronounced change in the stability of the current transients occurs at −0.578 V vs. SHE, and two clearly resolved regions are observed showing that 2-propanol is oxidized through different mechanisms at potentials below and above −0.578 V vs. SHE. This interpretation is consistent with previous studies that proposed that an oxidative dehydrogenation of 2-propanol to acetone occurs at low potentials, and that a slower

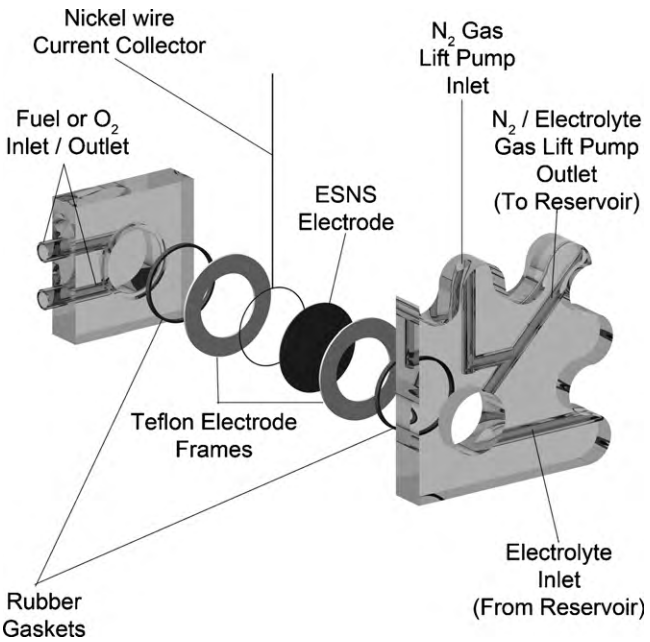

Fig. 1. Exploded and cut-away partial representation of the liquid electrolyte fuel cell (QuickCell^{TM} QC200) used in this study. One electrode-gasket-flow field assembly, and the electrolyte reservoir, is omitted for clarity. The active area of the electrodes was 5 cm^2. The electrolyte reservoir contained ∼200 mL of the 5 M KOH electrolyte and was maintained at 70 °C. The volume of electrolyte between the electrodes was ∼7.5 mL, and the volume of the anode/cathode chambers was ∼5.0 mL.

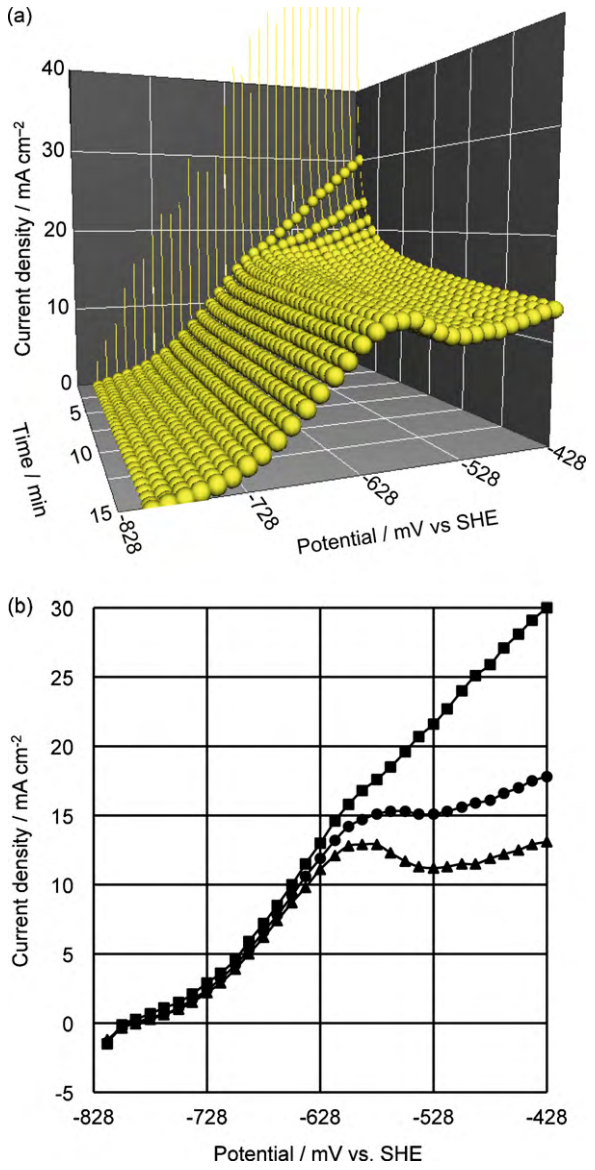

Fig. 2. (a) Current–time–potential profile for the half-cell oxidation of 1 M 2-propanol/1 M KOH over a 0.6 mg_{Pt} cm^{-2} ESNS electrode at 60 °C. The electrode was first conditioned at −928 mV vs. SHE for 2 min, then potentiostatic transients were collected for 15 min every 12.5 mV and plotted against the applied potential. The electrode was conditioned at −928 mV vs. SHE for 2 min between potential steps. (b) Current–potential curves at 0.5 min (■)), 3 min (●), and 15 min (▲) from Fig. 2(a). RHE = −828 mV vs. SHE.

oxidation to form CO_2 occurs at higher potentials [29,30]. To investigate how these different mechanisms impact the performance of an AD2PFC, fuel cells were built and characterized using this electrode material as the anode and cathode.

Fig. 4 shows the performance curves of the same ADAFC operating on 2-propanol, methanol, and hydrogen when polarized to a lower cell voltage limit of 0.5 V. The hydrogen cell is provided to gauge the performance of the cell hardware and the low platinum loading electrodes. The OCV of the AD2PFC is ∼160 mV higher than the ADMFC, and maintains a higher cell potential (electrical efficiency) at current densities up to 16 mA cm^{-2}. The performance of the ADMFC quickly degrades when the cell potential is cycled between its OCV and a lower cell voltage limit of 0.5 V. This degradation is presumably due to the accumulation of CO-like intermediates, and/or carbonate species, that inhibit the electrocatalyst. In contrast, the AD2PFC is stable to potential cycling

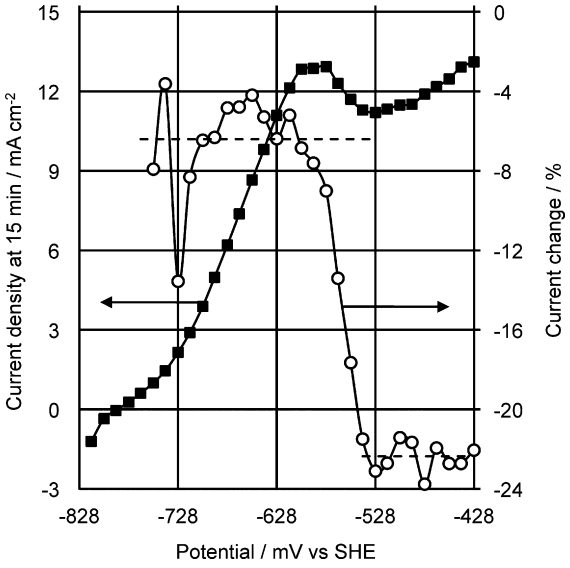

Fig. 3. Plot of the current density obtained at 15 min for the oxidation of 1 M 2-propanol/1 M KOH over a 0.6 mg_{Pt} cm^{-2} ESNS electrode at 60 °C (■), and the percentage of the current changed prior to the reported current (○). Points below −792 mV vs. SHE are omitted due to the large error associated with the small current density changes. RHE = −828 mV vs. SHE.

within this potential range, showing that 2-propanol does not significantly accumulate intermediates or carbonates that poison the catalyst under these conditions. To determine the contributions of the anodic and cathodic polarizations on the AD2PFC's polarization, the loadings of electrocatalyst were increased and studied in the AD2PFC and in 3-electrode experiments.

Fig. 5(a) shows the *j*–*t*–*E* profiles for the electro-oxidation of 2-propanol in 3-electrode experiments with commercial electrode having platinum loadings of 0.6 (10% platinum on Vulcan XC-72) and 1.5 mg cm^{-2} (20% platinum on Vulcan XC-72). Fig. 5(b) shows the current observed at 0.5 min, 3 min, and 15 min vs. the applied potential for both electrodes. Somewhat higher current densities

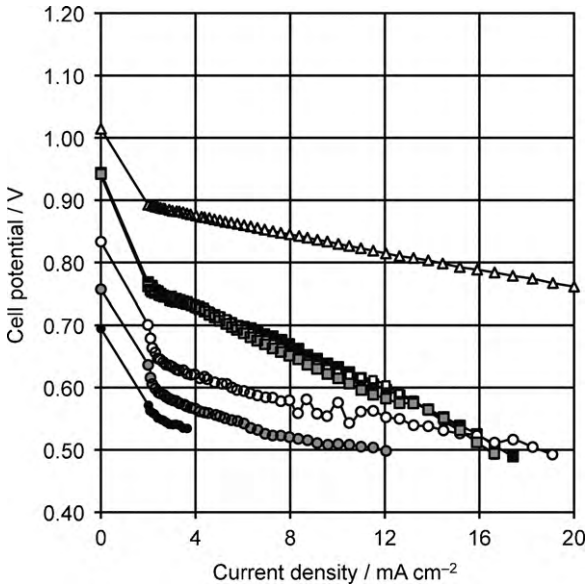

Fig. 4. Polarization curves for the same alkaline fuel cell operating on hydrogen (□), 100% 2-propanol (□ = first cycle, ■ = second cycle, ■ = third cycle), and 100% methanol (○ = first cycle, ● = second cycle, ● = third cycle). Temperature = 70 °C; alcohol flow rate = 0.5 mL min^{-1}; dry O_2 = 300 sccm; dry H_2 = 600 sccm; anode and cathode = 0.6 mg_{Pt} cm^{-2} ESNS electrode.

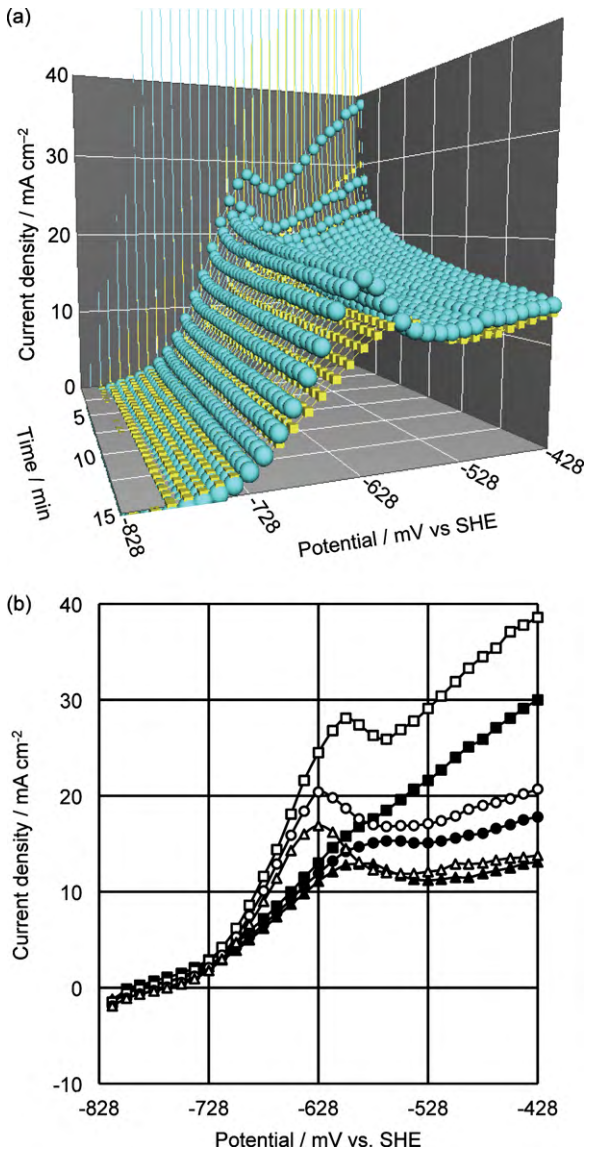

Fig. 5. (a) Current–time–potential profile for the half-cell oxidation of 1 M 2-propanol/1 M KOH over a 0.6 mg_{Pt} cm^{-2} ESNS electrode (cubes) or a 1.5 mg_{Pt} cm^{-2} ESNS electrode (spheres) at 60 °C. The electrode was first conditioned at −928 mV vs. SHE for 2 min, then potentiostatic transients were collected for 15 min every 12.5 mV and plotted against the applied potential. The electrode was conditioned at −928 mV vs. SHE for 2 min between potential steps. (b) Current–potential curves at 0.5 min (□,■)), 3 min (○,●), and 15 min (△,▲) from Fig. 5(a); 0.6 mg_{Pt} cm^{-2} = filled markers, 1.5 mg_{Pt} cm^{-2} = hollow markers. RHE = −828 mV vs. SHE.

occurred at lower potentials over the higher loading electrode. At 15 min, the *j*–*t*–*E* profile peaks at 16.9 mA cm^{-2} and −0.628 V vs. SHE over the 1.5 mg cm^{-2} electrode, and at 12.9 mA cm^{-2} and −0.578 V vs. SHE over the 0.6 mg cm^{-2} electrode. The current densities were similar for both electrodes at higher potentials (i.e., above −0.528 V vs. SHE). Fig. 6 shows the performance curves of the AD2PFC with different platinum loadings at the anode and cathode when the cell potential is scanned from its OCV to a lower cell voltage limit of 0.5 V. Increasing the catalyst loading at both the anode and cathode increases the current densities throughout this potential range. Decreasing the loading of the anode back to 0.6 mg cm^{-2}, while leaving the cathode unchanged at 1.5 mg cm^{-2}, did not adversely affect the cell performance at low current densities. Thus, the cathode is the dominant source of polarization under these conditions. The higher anode loading, however, did result in slightly higher current densities at cell voltages near

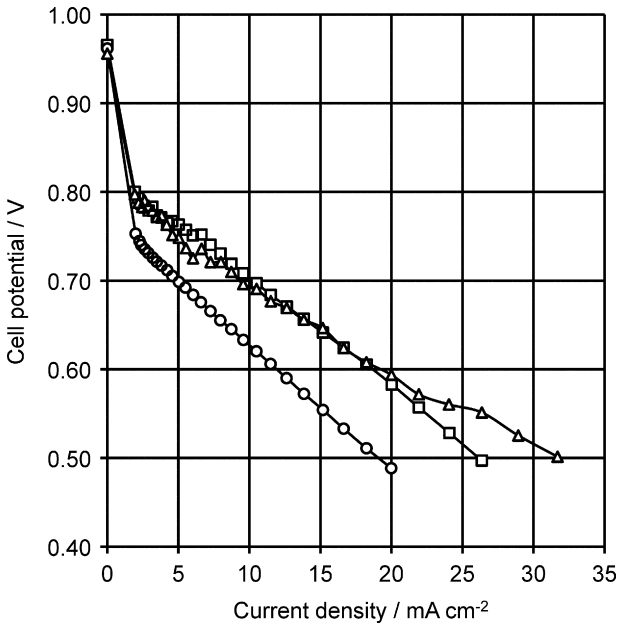

Fig. 6. Polarization curves for the AD2PFCs with differing anode and cathode electrocatalyst loadings. ○ = 0.6/0.6 mg_{Pt} cm^{-2}, □ = 0.6/1.5 mg_{Pt} cm^{-2}, ▯ = 1.5/1.5 mg_{Pt} cm^{-2} (anode loading/cathode loading). Temperature = 70 °C; alcohol flow rate = 0.5 mL min^{-1}; dry O_2 = 300 sccm.

0.5 V. This increase is consistent with the 3-electrode experiments (Fig. 5).

Fig. 7 shows the performance curves for the AD2PFC when cycled from its OCV to a lower cell voltage limit of 0 V. During the first cycle the maximum power density was 13.4 mW cm^{-2}; this power density is 2.4*X* that previously reported for AD2PFCs with higher loadings of electrocatalyst [31]. Polarizing the cell to a lower cell voltage limit of 0 V does, however, result in considerable performance degradation with cycling; the second cycle has a maximum power density that is 60% of the first cycle. This loss in activity is similar to the performance degradation observed during the polarization of the ADMFC to a lower cell voltage limit of 0.5 V

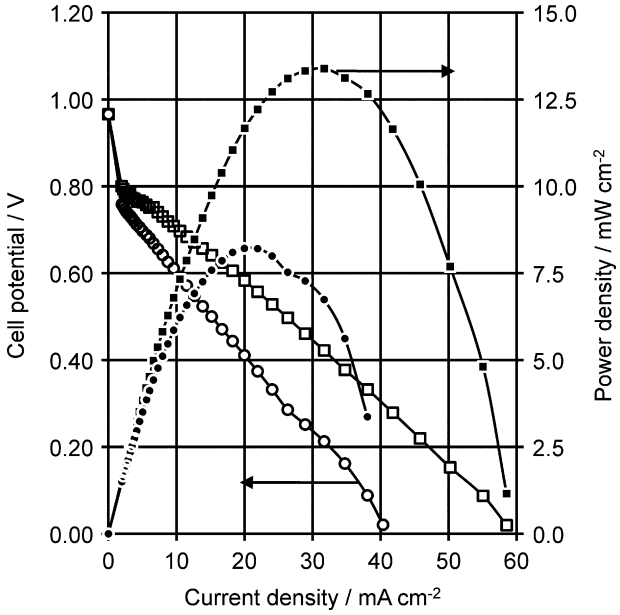

Fig. 7. Polarization (hollow markers) and power (filled markers) curves for the first (□,■) and second (○,●) polarization cycles of the AD2PFC to 0 V. Temperature = 70 °C; dry O_2 = 300 sccm; 100% 2-propanol = 0.5 mL min^{-1}; anode = 0.6 mg_{Pt} cm^{-2} ESNS electrode; cathode = 1.5 mg_{Pt} cm^{-2} ESNS electrode.

Table 1
Representative survey of ADAFC performance under comparable conditions.

Fuel	Anode (mg cm^{-2})	Cathode (mg cm^{-2})	Pressure[a] (MPa)	Electrolyte	Max power density (mW mg$_{anode\ cat}^{-1}$)	$E_{max\ power}$[b] (V)	Power at 0.5 V[b] (mW mg$_{anode\ cat}^{-1}$)	Temp (°C)	References
2 M MeOH/2 M KOH	PtRu/C (2.0)	Pt/C (1.0)	O_2 (0.2)	PBI	15.5	0.50	16.0	90	[14]
2 M EtOH/2 M KOH	PtRu/C (2.0)	Pt/C (1.0)	O_2 (0.2)	PBI	25.0	0.40	27.5	75	[18]
3 M EtOH/7 M KOH	HYPERMEC (1.0)	HYPERMEC (1.0)	99.7% O_2	Tokuyama A201	30.0	0.25	12.5	40	[19]
1 M EtOH/0.5 M KOH	PtRu (3.0)	Pt (3.0)	O_2	Tokuyama A201	20.0	0.25	4.2	60	[17]
10% EtOH/2 M KOH	Pd-(Ni-Zn)/C (1.0)	HYPERMEC (2.0)	O_2	Tokuyama A201	80.0	0.40	50.0	80	[16]
2 M MeOH/4 M NaOH	Pt/Ti (1.24)	Pt (0.77)	Air (0.1)	Morgane-ADP	10.6	0.30	2.8	60	[13]
2 M 2-PrOH/4 M KOH	PtRu (3.6)	MnO_2 (3.6)	Air (0.1)	PVA/TiO_2	1.5	0.30	16.0	25	[31]
2 M MeOH/2 M KOH	PtRu (3.6)	MnO_2 (3.6)	Air (0.1)	PVA/TiO_2	2.6	0.25	1.4	25	[31]
100% 2-PrOH	Pt/C (0.6)	Pt/C (1.5)	O_2 (0.1)	5 M KOH	22.3	0.42	22.0	70	This Work

[a] Missing values are due to unspecified pressures.
[b] Estimated values from published performance curves.

(Fig. 4). We note, however, that the stable power density achieved when the cell was polarized to a lower cell voltage limit of 0.5 V was 13.1 mW cm^{-2}: 98% of that achieved during the first polarization cycle to a lower cell voltage limit of 0 V. Thus, the change in mechanism at low and high anode potentials results in dramatic changes in the polarization characteristics of the AD2PFC. When the potential of the anode remains below the low-potential current maximum, the AD2PFC is capable of supplying relatively high power densities that are stable to potential cycling. When the cell is polarized to low cell potentials strongly bound intermediates form on the anode, and the performance of the AD2PFC declines.

Table 1 provides a representative survey of recently reported ADAFCs under comparable conditions. The catalyst-normalized AD2PFC performance is comparable to the state-of-the-art ADAFCs that operate on methanol or ethanol fuel. The AD2PFC's performance reported here is outperformed only by three recently reported ADEFCs.

4. Conclusions

These proof-of-concept AD2PFC investigations show a good correlation between the activity of the anode in 3-electrode experiments and the activity of the cell. Specifically, the AD2PAFC significantly outperformed the ADMFC, and it was more stable when the cell potential was kept above 0.5 V. At lower cell voltages, the maximum power density was only marginally higher, and the cell was unstable, presumably due to anode poisoning by carbonates or strongly adsorbed intermediates from acetone oxidation. The major source of polarization is likely the cathode when these cells operate reversibly at relatively high voltages. The performance of these cells is promising and suggests that a carefully optimized polymer based system will provide high power densities in the absence of non-electrochemical reactions that consume hydroxide at the anode (i.e., carbonate formation). Such studies are currently underway in these laboratories.

Acknowledgments

We thank the Natural Sciences and Engineering Research council of Canada and the University of Alberta for supporting this research.

References

[1] J.R. Varcoe, R.C.T. Slade, Fuel Cells 5 (2) (2005) 187–200.
[2] E. Antolini, E.R. Gonzalez, J. Power Sources 195 (11) (2010) 3431–3450.
[3] J.S. Spendelow, A. Wieckowski, Phys. Chem. Chem. Phys. 9 (21) (2007) 2654–2675.
[4] K. Matsuoka, Y. Iriyama, T. Abe, M. Matsuoka, Z. Ogumi, J. Power Sources 150 (2005) 27–31.
[5] H. Bunazawa, Y. Yamazaki, J. Power Sources 182 (1) (2008) 48–51.
[6] H. Bunazawa, Y. Yamazaki, J. Power Sources 190 (2) (2009) 210–215.
[7] R.S. Jayashree, D. Egas, J.S. Spendelow, D. Natarajan, L.J. Markoski, P.J.A. Kenis, Electrochem. Solid-State Lett. 9 (5) (2006) A252–A256.
[8] J. Kim, T. Momma, T. Osaka, J. Power Sources 189 (2) (2009) 999–1002.
[9] C.C. Yang, J. Membr. Sci. 288 (1–2) (2007) 51–60.
[10] C.C. Yang, S.J. Chiu, W.C. Chien, J. Power Sources 162 (1) (2006) 21–29.
[11] C.C. Yang, S.J. Chiu, C.T. Lin, J. Power Sources 177 (1) (2008) 40–49.
[12] C.C. Yang, C.T. Lin, S.J. Chiu, Desalination 233 (1–3) (2008) 137–146.
[13] E.H. Yu, K. Scott, J. Appl. Electrochem. 35 (1) (2005) 91–96.
[14] H.Y. Hou, G.Q. Sun, R.H. He, B.Y. Sun, W. Jin, H. Liu, Q. Xin, Int. J. Hydrogen Energy 33 (23) (2008) 7172–7176.
[15] V. Bambagioni, C. Bianchini, A. Marchionni, J. Filippi, F. Vizza, J. Teddy, P. Serp, M. Zhiani, J. Power Sources 190 (2) (2009) 241–251.
[16] C. Bianchini, V. Bambagioni, J. Filippi, A. Marchionni, F. Vizza, P. Bert, A. Tampucci, Electrochem. Commun. 11 (5) (2009) 1077–1080.
[17] N. Fujiwara, Z. Siroma, S.I. Yamazaki, T. Ioroi, H. Senoh, K. Yasuda, J. Power Sources 185 (2) (2008) 621–626.
[18] H. Hou, G. Sun, R. He, Z. Wu, B. Sun, J. Power Sources 182 (1) (2008) 95–99.
[19] Y.S. Li, T.S. Zhao, Z.X. Liang, J. Power Sources 187 (2) (2009) 387–392.
[20] Y.S. Li, T.S. Zhao, Z.X. Liang, J. Power Sources 190 (2) (2009) 223–229.

[21] A.D. Modestov, M.R. Tarasevich, A.Y. Leykin, V.Y. Filimonov, J. Power Sources 188 (2) (2009) 502–506.
[22] C.C. Yang, Y.J. Lee, S.J. Chiu, K.T. Lee, W.C. Chien, C.T. Lin, C.A. Huang, J. Appl. Electrochem. 38 (10) (2008) 1329–1337.
[23] C. Xu, Z. Tian, Z. Chen, S.P. Jiang, Electrochem. Commun. 10 (2) (2008) 246–249.
[24] Y. Su, C. Xu, J. Liu, Z. Liu, J. Power Sources 194 (1) (2009) 295–297.
[25] J. Lu, S. Lu, D. Wang, M. Yang, Z. Liu, C. Xu, S.P. Jiang, Electrochim. Acta 54 (23) (2009) 5486–5491.
[26] J. Ye, J. Liu, C. Xu, S.P. Jiang, Y. Tong, Electrochem. Commun. 9 (12) (2007) 2760–2763.
[27] J. Liu, J. Ye, C. Xu, S.P. Jiang, Y. Tong, J. Power Sources 177 (1) (2008) 67–70.
[28] L.N. Menard, S.H. Bergens, J. Power Sources 194 (1) (2009) 298–302.
[29] M.E.P. Markiewicz, D.M. Hebert, S.H. Bergens, J. Power Sources 161 (2) (2006) 761–767.
[30] M.E.P. Markiewicz, S.H. Bergens, J. Power Sources 185 (1) (2008) 222–225.
[31] C.C. Yang, S.J. Chiu, K.T. Lee, W.C. Chien, C.T. Lin, C.A. Huang, J. Power Sources 184 (1) (2008) 44–51.